

Article

Transmission Electron Microscopy Investigations on a Polysiloxane Preceramic Polymer Pyrolyzed at High Temperature in Argon

Sébastien Vry ¹, Marilyne Roumanie ¹, Richard Laucournet ¹ and Guillaume Bernard-Granger ^{2,*}

¹ CEA, LITEN, DTNM, Université Grenoble Alpes, 38000 Grenoble, France; sebastien.vry@cea.fr (S.V.); marilyne.roumanie@cea.fr (M.R.); richard.laucournet@cea.fr (R.L.)

² CEA, DES, ISEC, DMRC, Université Montpellier, 30200 Marcoule, France

* Correspondence: guillaume.bernard-granger@cea.fr

Received: 27 July 2020; Accepted: 30 September 2020; Published: 3 October 2020



Abstract: A commercially available methylphenylvinylhydrogen polysiloxane preceramic polymer was cross-linked and pyrolyzed in argon in order to study if this compound could be used as an organic precursor for the manufacture of silicon carbide parts by photopolymerisation-based three-dimensional printing. X-Ray diffraction experiments and transmission electron microscopy observations showed that the pyrolyzed material was constituted by an interconnected polycrystalline network made of faulted/twinned β -SiC grains surrounded by an amorphous and porous second phase mainly constituted (at least 80 at%) of carbon. The free carbon residual content was estimated to be around 17.2 wt%. Additional efforts are then required to be able to use such a preceramic polymer to manufacture SiC parts by photopolymerisation-based three-dimensional printing.

Keywords: polymer-derived-ceramics; SiC; microstructure

1. Introduction

Polycrystalline silicon carbide ceramics (SiC) are materials of choice for different kinds of applications, for example armors for infantrymen, vehicles and helicopter pilot seats [1,2] where high hardness and compressive strength values are required in conjunction with a low density. Polycrystalline SiC is also an interesting structural material for high temperature applications, as for example kiln elements and heat exchangers, where resistance to oxidation [3] and creep [4,5] are needed. Several hundred polytypes of SiC have been identified, ranging from purely hexagonal 2H-SiC to purely cubic 3C-SiC [6]. However, the polytypes which have received the most attention are 6H-SiC (α -SiC, hexagonal, space group $P6_3mc$, $a \approx 3.08$ Å and $c \approx 15.12$ Å), 3C-SiC (β -SiC, cubic, space group $F\bar{4}3m$, $a \approx 4.36$ Å) and 4H-SiC (α -SiC, hexagonal, space group $P6_3mc$, $a \approx 3.08$ Å and $c \approx 10.05$ Å) [6].

When the shape of the final object is plain and/or simple, industrial manufacturing of polycrystalline SiC ceramics is based on a powder metallurgy approach, where a green part (obtained typically using uniaxial-pressing or slip casting) is sintered at high temperature in a non-oxidizing atmosphere. Most of the time, to obtain a closed porosity after sintering, a certain amount of additives (Y_2O_3 - Al_2O_3 [7] or B-C [8], for example) are incorporated into the formulation to decrease, as much as possible, the required temperature.

For objects with complex shapes and manufactured using a standard powder metallurgy process, machining steps from the green and/or fired states are mandatory. This takes time, it is expensive, and a non-negligible fraction of the original material is removed and unusable. Additive manufacturing processes overcome these drawbacks. Among additive manufacturing processes,

the photopolymerisation-based printing (stereolithography: SLA; digital light processing: DLP; lithography-based ceramics manufacturing: LCM) is a well-known technology to shape complex polycrystalline ceramic parts [9]. To print a given part, a photocurable organic formulation, containing an optimized volume fraction of the ceramic particles of interest, is submitted layer by layer to an UV LED (wavelength is typically 365 nm) exposure during a short period of time.

The complex refractive index of the 6H α -SiC polytype has been computed for a wavelength set to 365 nm (no data have been found for β -SiC in this wavelength range) and is given roughly (no distinction between the ordinary and extraordinary values, α -SiC is birefringent due to its non-cubic crystalline structure) by $N = 2.7 - 0.1i$, where $n = 2.7$ and $k = 0.1$ are the real and imaginary parts, respectively [10]. The difference in the real part of the refractive index (Δn) between a photocurable organic formulation (typically in the range from 1.6 to 1.9 for a wavelength close to 365 nm [11]) and embedded SiC particles leads to a significant diffusion phenomenon when insulating by a UV LED. Moreover, the significant value of the imaginary part of the refractive index of 6H α -SiC grains also leads to UV light absorption. Such optical interactions strongly inhibit the photopolymerization of the organic formulation containing SiC particles, even for solid loadings below 10 vol% [12]. Recently, a photocurable resin containing 40 vol% of SiC particles has been elaborated and photopolymerization inhibition was overcome [13]. However, multiple infiltration and polymer burnout steps are required to reduce as much as possible the residual porosity [13].

To solve this problem the use of preceramic polymers is a solution of choice. Polysilazanes ($[-\text{SiR}^1\text{R}^2-\text{NR}^3]_n$, R^1 , R^2 and R^3 may represent hydrogen atoms or organic substituents), polycarbosilanes ($[\text{R}^1\text{R}^2\text{Si}-\text{CH}_2]_n$) and polysiloxanes ($[\text{R}^1\text{R}^2\text{Si}-\text{O}]_n$) are silicon-based polymers leading to a wide range of ceramics after pyrolysis (SiC, SiCN, SiOC, or even quaternary compounds) and belonging to the polymer-derived ceramics (PDC) generic family [14]. The main advantages of using such polymers to manufacture SiC parts are that they are miscible in photocurable organic formulations and that they have a much lower UV light-absorbance than SiC particles for a tridimensional construction using photopolymerisation-based printing.

Polycarbosilanes are the suitable candidates to obtain SiC/SiOC ceramics after pyrolysis [15]. However, these organometallic polymers are expensive and oxygen sensitive. Thus, polysiloxanes are seen as alternative compounds [16,17]. As an example, polysiloxanes have already been used in order to form Åkermanite ($\text{Ca}_2\text{MgSi}_2\text{O}_7$) reticulated scaffolds by DLP [17]. Accordingly, the objective of the work reported in this paper was to investigate the microstructure developed after pyrolysis of a cross-linked commercially-available polysiloxane compound. The results will constitute the basis for further developments of an organic formulation containing such a PDC that will be photocurable and three-dimensionally printable using photopolymerisation-based printing.

2. Materials and Methods

The commercial Silres H62C (Wacker-Chemie AG) methylphenylvinylhydrogen polysiloxane preceramic polymer was used. It is liquid at room temperature and was cross-linked in air, at 200 °C, for 1 h (heating rate set to 2 °C/min). Then a pyrolysis treatment was performed in argon, at 1700 °C, during 1 h (heating rate set to 1 °C/min).

After pyrolysis, chemical analyses of carbon, oxygen and hydrogen contents were determined by instrumental gas analysis (IGA, CS744 and ONH836 equipments, Leco, Carbon-ISO21068, Oxygen-DIN EN 10276). The silicon content was measured by inductively coupled plasma atomic emission spectroscopy (ICP-OES, Arcos 2, Spectro, DIN 51008-2 and DIN 51009).

The crystallization behavior of the pyrolyzed material was characterized by X-ray diffraction (XRD, Bruker D8 Advance, LynxEye detector with Cu-K α radiations, the K- α_2 line was not removed). EVA Software (Bruker) and the JCPDS (Joint Committee on Powder Diffraction Standards) database were used to identify crystalline phases.

From the pyrolyzed material, a thin foil was prepared using focused ion beam (FIB, Strata DB 235, FEI). Then transmission electron microscopy (TEM) and scanning transmission electron microscopy

(STEM, a high angle annular dark field—HAADF—detector is used) observations (Tecnai Osiris, FEI, acceleration voltage of 200 kV, point to point resolution of 2.5 Å) coupled to energy dispersive spectroscopy analyses (EDS, Esprit, Bruker) using four quadrant silicon drift detectors (ChemiStem technology, FEI) were performed.

3. Results and Discussion

Results from IGA and ICP analyses on the pyrolyzed cross-linked material gives the following composition (95% confidence level, $k = 2$): 37.00 ± 0.48 at% Si— 0.41 ± 0.03 at% O— 62.41 ± 0.44 at% C— 0.18 ± 0.02 at% H which reduces to $\text{SiO}_{0.011}\text{C}_{1.687}\text{H}_{0.005}$. According to Crespiera, it is possible to calculate the phase composition by assuming that only Si-O, Si-C bonds and residual free carbon (the hydrogen contribution is neglected) are present in the pyrolyzed material [18], which gives: 82.15 wt% SiC—0.69 wt% SiO—17.16 wt% C_{free} . The content of residual carbon is not negligible.

Figure 1 shows the XRD pattern acquired on the pyrolyzed cross-linked material. Main peaks are related to the cubic β -SiC phase. The minor reflexion, marked by a star for a 2θ value of 33.7° , may be explained by the presence of faults in the regular cubic stacking sequences of the β -SiC individual grains constituting the pyrolyzed sample, as reported by Pujar [19].

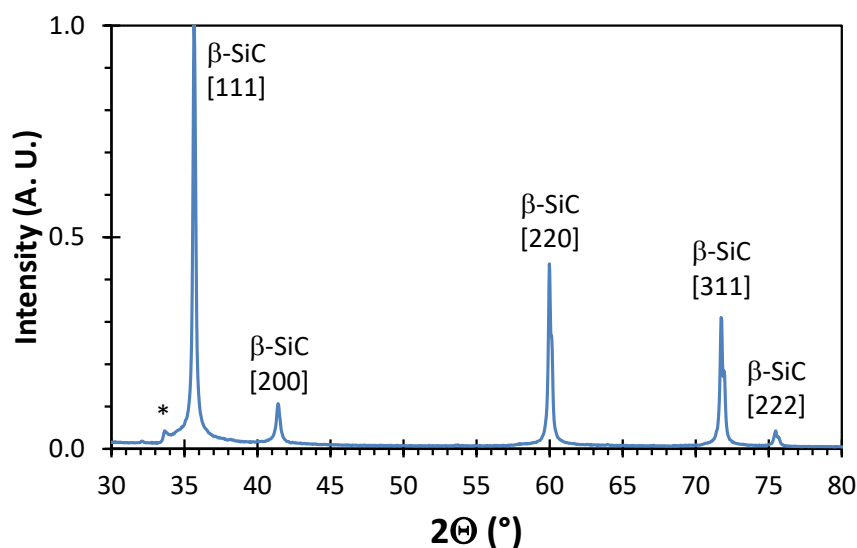


Figure 1. XRD pattern acquired on a cross-linked and pyrolyzed methylphenylvinylhydrogen polysiloxane preceramic polymer sample.

Figure 2a shows a STEM/HAADF general view of the pyrolyzed cross-linked material. A bright polycrystalline interconnected network surrounded by a vermicular dark second-phase is observed. Because the intensity of the signal detected by a HAADF detector is proportional to the atomic number power 1.7 (Z-contrast), a bright object is constituted by heavy elements. Accordingly, the dark second-phase is constituted by pores and/or lighter elements than the ones constituting the bright polycrystalline network.

Figure 2b shows a STEM/HAADF view at a higher magnification and Figure 2c–e show EDS maps for the Si, C and O associated chemical elements, respectively. The grains constituting the polycrystalline network contain Si, C and O elements. Local chemical quantifications from EDS analyses carried out in point-mode have been performed using the Cliff–Lorimer method with theoretical k -factors calculated under Esprit software for an acceleration voltage of 200 kV (thin foil thickness assumed to be 75 nm). The composition obtained for some crystalline grains is 50.12 ± 0.22 at% Si— 48.69 ± 1.64 at% C— 0.82 ± 0.07 at% O— 0.36 ± 0.04 at% Al. Accordingly, the network is made of slightly oxidized SiC grains that are enriched in Al, this last element being a process impurity from the furnace used. Indeed, aluminum is a well-known p-type effective dopant for SiC in the semiconductors

industry [6]. Most of the grains exhibit also stacking faults/twins, as shown on Figure 2a, which is compatible with the cubic β crystallographic structure identified by XRD. The dark second-phase surrounding the polycrystalline network is porous, contains C and O elements and is devoid of Si. Using EDS analyses, its average composition has been determined to be 7.92 ± 0.19 at% Si— 80.86 ± 2.95 at% C— 11.00 ± 0.49 at% O— 0.21 ± 0.04 at% P. It is strongly enriched in C and also contains P as another process impurity related to the furnace used. Such an oxygen content around 11.00 at% is possibly in relation to entrapped gaseous silicon monoxide. Indeed, gaseous silicon monoxide is known to form during the carboreduction of SiO_2 in presence of carbon [20]. The formation of crystalline SiC generally takes place when the molar ratio of silica to carbon is over one to three. Before the total completion into SiC and when the molar ratio of silica to carbon reaches 1:1, silicon monoxide could be produced and entrapped into the carbon rich phase during the cooling step of the pyrolysis treatment, according to the reaction $\text{SiO}_2(\text{s}) + \text{C}(\text{s}) \rightarrow \text{SiO}(\text{g}) + \text{CO}(\text{g})$. Finally, the EDS map related to the O element (Figure 2e) is also interesting because it shows an oxygen enrichment at the periphery of the SiC grains.

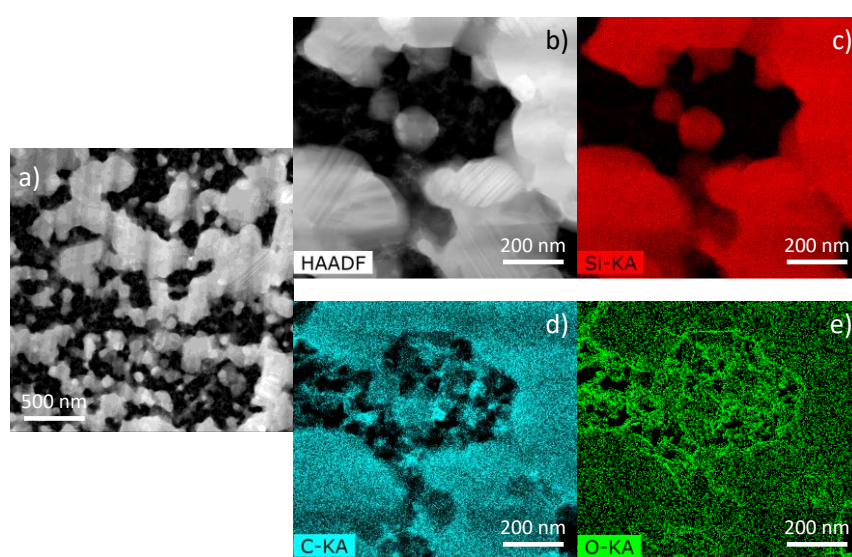


Figure 2. (a) STEM/HAADF general view of the cross-linked and pyrolyzed methylphenylvinylhydrogen polysiloxane preceramic polymer sample; (b) Detailed view in STEM/HAADF mode; (c) Associated EDS map for Si; (d) Associated EDS map for C; (e) Associated EDS map for O. STEM: scanning transmission electron microscopy; HAADF: high angle annular dark field; EDS: energy dispersive spectroscopy.

Figure 3a is a bright-field general view in TEM mode of the pyrolyzed cross-linked sample. The polycrystalline network made of faulted/twinned grains (all the grains exhibit such contrasts when tilted under the electron beam) are surrounded by a fluffy second phase. Figure 3b has been acquired at a higher magnification, always using the bright field TEM mode. The faulted/twinned structure of the individual SiC grains is clear and the fluffy phase is constituted itself by a porous structure of interconnected and tortuous filaments.

Figure 4a is a HRTEM (high resolution transmission electron microscopy) view of a crystalline SiC grain at its surface vicinity. Lattice fringes are clearly visible in the bulk of the grain and a fuzzy disordered arrangement is present at its surface. Figure 4b shows that such a layer is enriched in O in comparison to the bulk of the grain, as it was already observed at a lower magnification (Figure 2e). This layer results possibly from surface oxidation of the silicon carbide grain and is probably made of SiO_2 . A fast Fourier transform (FFT) of the HRTEM image focusing on the layer shows that it has an amorphous nature (Figure 4c). Performing a FFT of the HRTEM image focusing on the core of the grain enables an indexation compatible with the β -SiC cubic structure (Figure 4d), in agreement to the XRD results. By selecting the $(\bar{2}00)$ crystallographic direction for β -SiC and doing an inverse FFT

shows stacking faults and dislocations in the core of the grain (Figure 4e). Additional observations using the HRTEM mode show also that the fluffy second phase surrounding the polycrystalline β -SiC grains is amorphous (not shown here).

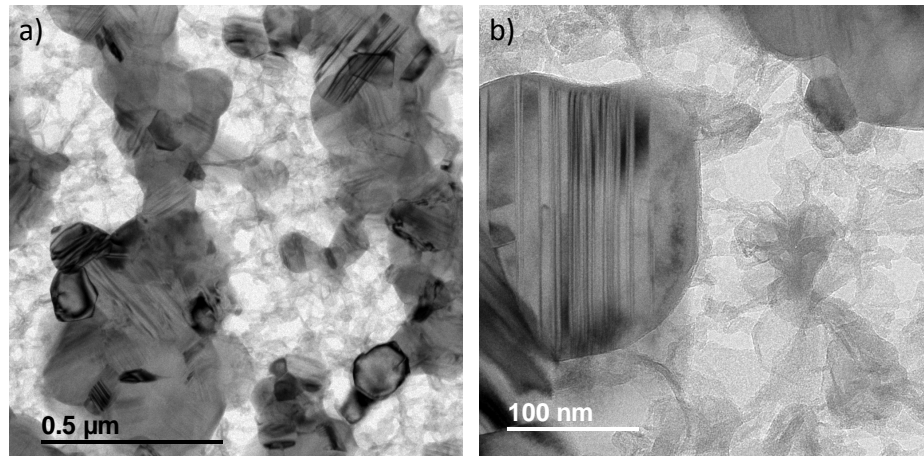


Figure 3. (a) Transmission electron microscopy (TEM) view in bright field mode of the cross-linked and pyrolyzed methylphenylvinylhydrogen polysiloxane preceramic polymer sample; (b) Detailed view in bright field TEM mode.

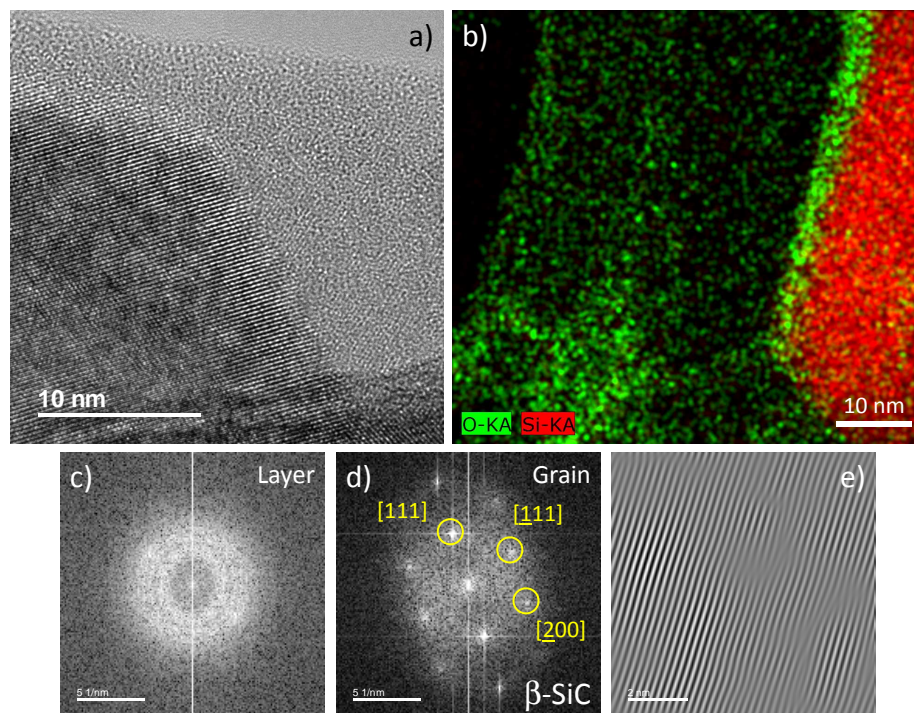


Figure 4. (a) High resolution transmission electron microscopy (HRTEM) view close to the surface of a silicon carbide grain showing the presence of a thin layer; (b) Combined EDS maps for Si and O showing that the surface layer of silicon carbide grains is enriched in oxygen; (c) fast Fourier transform (FFT) on the surface layer; (d) FFT in the core of the silicon carbide grain; (e) Inverse FFT using the $(\bar{2}00)$ direction of the silicon carbide grain.

4. Conclusions

After cross-linking at 200 °C and pyrolysis at 1700 °C in argon, a commercially available methylphenylvinylhydrogen polysiloxane preceramic polymer gives a solid compound made of 82.15 wt% SiC, 0.69 wt% SiO₂ and 17.16 wt% of free C.

X-Ray diffraction experiments and transmission electron microscopy observations show that the pyrolyzed material is constituted by an interconnected polycrystalline network made of faulted/twinned β -SiC grains surrounded by an amorphous and porous second phase mainly constituted (at least 80 at%) of carbon. An amorphous thin layer enriched in oxygen is present at the surface of the β -SiC grains. It results possibly from the SiC grains surface oxidation during processing.

To improve the SiC conversion yield in the future, additional tests will be completed by increasing the pyrolysis temperature and/or by adding a small fraction of free silicon, for example. Additional work will also focus on the development of an organic formulation, integrating the methylphenylvinylhydrogen polysiloxane preceramic polymer, devoted to be cured and three-dimensionally printed using stereolithography.

Author Contributions: Conceptualization: S.V., M.R., R.L. and G.B.-G.; Methodology: S.V., M.R. and G.B.-G.; Formal analysis: S.V., M.R. and G.B.-G.; Investigation: S.V.; Writing—original draft preparation: S.V., M.R., R.L. and G.B.-G.; Supervision: M.R., R.L. and G.B.-G. All authors have read and agreed to the published version of the manuscript.

Funding: This research received no external funding.

Conflicts of Interest: The authors declare no conflict of interest.

References

1. Zinszner, J.L.; Forquin, P.; Rossiquet, G. Experimental and numerical analysis of the dynamic fragmentation in a SiC ceramic under impact. *Int. J. Impact Eng.* **2015**, *76*, 9–19. [[CrossRef](#)]
2. Forquin, P.; Rossiquet, G.; Zinszner, J.L.; Erzar, B. Microstructure influence on the fragmentation properties of dense silicon carbides under impact. *Mech. Mater.* **2018**, *123*, 59–76. [[CrossRef](#)]
3. Jensen, R.P.; Luecke, W.E.; Padture, N.P.; Wiederhorn, S.M. High-temperature properties of liquid-phase-sintered α -SiC. *Mater. Sci. Eng.* **2000**, *A282*, 109–114. [[CrossRef](#)]
4. Melendez-Martinez, J.J.; Castillo-Rodriguez, M.; Dominguez-Rodriguez, A.; Ortiz, A.L.; Guiberteau, F. Creep and microstructural evolution at high temperature of liquid phase-sintered silicon carbide. *J. Am. Ceram. Soc.* **2007**, *90*, 163–169. [[CrossRef](#)]
5. Lara, F.; Munoz, A.; Castillo-Rodriguez, M.; Dominguez-Rodriguez, A. High-temperature compressive creep of spark-plasma sintered additive-free polycrystalline β -SiC. *J. Eur. Ceram. Soc.* **2012**, *32*, 3445–3451. [[CrossRef](#)]
6. Park, Y.S. *SiC Materials and Devices*; Academic Press: Chesnut Hill, UK, 1998.
7. Omori, M.; Takei, H. Pressureless sintering of SiC. *J. Am. Ceram. Soc.* **1982**, *65*, C92. [[CrossRef](#)]
8. Prochazka, S.; Scanlan, R.M. Effect of boron and carbon on sintering of SiC. *J. Am. Ceram. Soc.* **1975**, *58*, 72. [[CrossRef](#)]
9. Travitzky, N.; Bonet, A.; Dermeik, B.; Fey, T.; Filbert-Demut, I.; Schlier, L.; Schlordt, T.; Greil, P. Additive manufacturing of ceramic-based materials. *Adv. Eng. Mater.* **2014**, *16*, 729–754. [[CrossRef](#)]
10. Pegourié, B. Optical properties of α silicon carbide. *Astronom. Astrophys.* **1988**, *194*, 335–339.
11. Nalwa, H.S.; Miyata, S. *Nonlinear Optics of Organic Molecules and Polymer*; CRC Press Inc.: Boca Raton, FL, USA, 1997.
12. Badev, A.; Abouliatim, Y.; Chartier, T.; Lecamp, L.; Lebaudy, P.; Chaput, C.; Delage, C. Photopolymerization kinetics of a polyether acrylate in the presence of ceramic fillers used in stereolithography. *J. Photochem. Photobiol. A Chem.* **2011**, *222*, 117–122. [[CrossRef](#)]
13. He, R.; Ding, G.; Zhang, K.; Li, Y.; Fang, D. Fabrication of SiC Ceramic architectures using stereolithography combined with precursor infiltration and pyrolysis. *Ceram. Int.* **2019**, *45*, 14006–140014. [[CrossRef](#)]
14. Colombo, P.; Mera, G.; Riedel, R.; Soraru, G.D. Polymer-derived ceramics: 40 years of research and innovation in advanced ceramics. *J. Am. Ceram. Soc.* **2010**, *93*, 1805–1837. [[CrossRef](#)]
15. De Hazan, Y.; Penner, D. SiC and SiOC ceramic articles produced by stereolithography of acrylate modified polycarbosilane systems. *J. Eur. Ceram. Soc.* **2017**, *37*, 5205–5212. [[CrossRef](#)]
16. Schmidt, J.; Colombo, P. Digital light processing of ceramic components from polysiloxanes. *J. Eur. Ceram. Soc.* **2018**, *38*, 57–66. [[CrossRef](#)]

17. Dasana, A.; Elsayed, H.; Kraxnera, J.; Galusekd, D.; Colombo, P.; Bernardo, E. Engineering of silicone based mixtures for the digital light processing of Åkermanite scaffolds. *J. Eur. Ceram. Soc.* **2020**, *40*, 2566–2572. [[CrossRef](#)]
18. Martinez-Crespiera, S.; Ionescu, E.; Kleebe, H.J.; Riedel, R. Pressureless synthesis of fully dense and crack-free SiOC bulk ceramics via photo-crosslinking and pyrolysis of a polysiloxane. *J. Eur. Ceram. Soc.* **2011**, *31*, 913–919. [[CrossRef](#)]
19. Pujar, V.V.; Cawley, J.D. Effect of stacking faults on the X-ray diffraction profiles of β -SiC powders. *J. Am. Ceram. Soc.* **1995**, *78*, 774–782. [[CrossRef](#)]
20. Miller, P.D.; Lee, J.G.; Cutler, I.B. The reduction of silica with carbon and silicon carbide. *J. Am. Ceram. Soc.* **1979**, *62*, 147–149. [[CrossRef](#)]



© 2020 by the authors. Licensee MDPI, Basel, Switzerland. This article is an open access article distributed under the terms and conditions of the Creative Commons Attribution (CC BY) license (<http://creativecommons.org/licenses/by/4.0/>).